



## STUDY ON FRACTURE ASSESSMENT BY GTN MODEL ANALYSIS FOR DISSIMILAR METAL WELD IN BWR REACTOR PRESSURE VESSEL COMPONENTS

Takuya Ogawa<sup>1</sup>, Shuichi Yoshida<sup>2</sup>, Takahiro Hayashi<sup>3</sup>, Masao Itatani<sup>2</sup>, Toshiyuki Saito<sup>2</sup>

<sup>1</sup> Specialist, Toshiba Energy Systems and Solutions Corporation, Yokohama, Japan  
(takuya4.ogawa@toshiba.co.jp)

<sup>2</sup> Toshiba Energy Systems and Solutions Corporation, Yokohama, Japan

<sup>3</sup> Fellow, Toshiba Energy Systems and Solutions Corporation, Yokohama, Japan

### ABSTRACT

Cases of stress corrosion cracking (SCC) in Ni-base alloy weld metals welded to the low alloy steel (LAS) of reactor pressure vessel (RPV) have led to discussions on the possibility of SCC propagation into the RPV. The Japan Society of Mechanical Engineers (JSME) Fitness-for-Service code provides fracture evaluation methodology based on linear elastic fracture mechanics for flaws in the RPV, assuming neutron irradiation in the RPV beltline region. It is considered, however, more rational methodology of fracture evaluation can be applied to the RPV such as a bottom head of boiling water reactor (BWR) since the effect of neutron irradiation is negligible. In the previous studies, the fracture mode of RPV material and dissimilar metal weld (DMW) consisted of Ni-base alloy weld metals and LAS has been investigated by using a large-scale, heavy forged steel part named “bottom head ring”, manufactured for a recent BWR. The authors reported that the results of fracture tests showed ductile failure and the fracture loads evaluated using the elastic-plastic fracture mechanics (EPFM) methodology have showed a good agreement with the maximum loads in the fracture tests on plate specimens with a semi-elliptical surface crack. Moreover, the authors reported that damage mechanics analysis by using Gurson-Tvergaard-Needleman (GTN) model can also be applied to the prediction of the fracture loads for the RPV material.

In the present study, the applicability of damage mechanics analysis by using the GTN model to fracture evaluation for DMW in a RPV bottom head of BWR was investigated. By comparison of the relationship between load and load-line displacement (LLD) obtained by the fracture toughness tests with that obtained by finite element analysis (FEA) using the GTN model, parameters of the GTN model were investigated and determined for heat affected zone (HAZ) of the weld as well as Ni-base alloy weld metals and LAS. Fracture analysis for the DMW plate specimen with a semi-elliptical surface flaw was performed by using the GTN model parameters determined. Relationship between load and crack mouth opening displacement (CMOD) was compared between the tests and analyses. As a result, the analyses showed good agreement with the test results. Consequently, the results obtained in the present study totally supported the applicability of the GTN model to the DMW in a RPV bottom head component.

### INTRODUCTION

In the nuclear power industry, stress corrosion cracking (SCC) in Ni-base alloy weld metals is an important issue (see Bamford et al. 2003, Matsunaga et al. 2003, Aoki et al. 2005, Bjurman et al. 2017 and NRC 2017). Cases of SCC in dissimilar metal weld (DMW) have led to discussions on the possibility of SCC propagation into low alloy steel (LAS) of reactor pressure vessel (RPV) and the potential impact on its structural integrity (see Bjurman et al. 2017 and NRC 2017). In the structural integrity assessment, the fracture evaluation for a flaw in a RPV is generally performed using the fracture evaluation methodology and plane strain fracture toughness ( $K_{Ic}$ ) criterion based on linear elastic fracture mechanics, such as provided in “Section XI of the ASME Code” in U.S. and “Rules on Fitness-for-Service for Nuclear Power Plants of the Japan Society of Mechanical Engineers Code (JSME FFS Code)” in Japan. The current fracture

evaluation methodology, however, was originally developed for preventing unstable, brittle fracture due to irradiation embrittlement of RPV materials where neutron irradiation damage accumulates during operation, causing decreases in ductility and fracture toughness, and where pressure and thermal loadings are expected at temperatures below the upper shelf temperature range. The acceptance criteria based on the elastic-plastic fracture mechanics (EPFM) methodology is also provided in ASME Code Case N-749 2012 (see Gustin et al. 2012) for flaws in ferritic components when the service temperature of the components is in the upper shelf temperature range. However, the fracture assessment methodology for DMW components, which takes into consideration the potential effect of DMW on the fracture behavior of LAS, has not been sufficiently studied and established. Note that for such DMW locations, the neutron irradiation damage is negligible, and the operating temperature is above the upper shelf temperature range in general.

In the previous studies (Hayashi et al. 2021 and 2022), the authors reported that the fracture loads evaluated using the EPFM methodology have showed a good agreement with the maximum loads in the fracture tests on plate specimens with a semi-elliptical surface crack. These results strongly support the applicability of fracture assessment methodology based on EPFM to the RPV material and the DMW of RPV bottom head components. Moreover, the authors have investigated the applicability of the GTN model to fracture evaluation for the RPV material and revealed that the GTN model can predict the load-crack mouth opening displacement (CMOD) relationship obtained in the fracture tests on plate specimens with a semi-elliptical surface crack (see Yoshida et al. 2022 and Ogawa et al. 2023). This paper summarizes the results of investigation for the applicability of the GTN model to the DMW of RPV bottom head components consisted of Ni-base alloy weld metal and LAS.

## TEST MATERIAL

The bottom head ring material is an ASME SA-508 Grade 3 Class 1 forging, formerly designated as SA-508 Class 3 in the old edition of the ASME code. The inner diameter is approximately 7100 mm and the thickness is approximately 250 mm at the thickest part in the product shape. The material had been quenched-tempered and post weld heat-treated. The post weld heat treatment temperature was approximately 600°C. The inner surface of the material has Alloy 82 cladding and weld buildup for the DMW joint between Alloy 600 of the shroud support and LAS of the RPV. Figure 1 shows schematic drawings of RPV bottom head component and test material with H9 weld buildup.

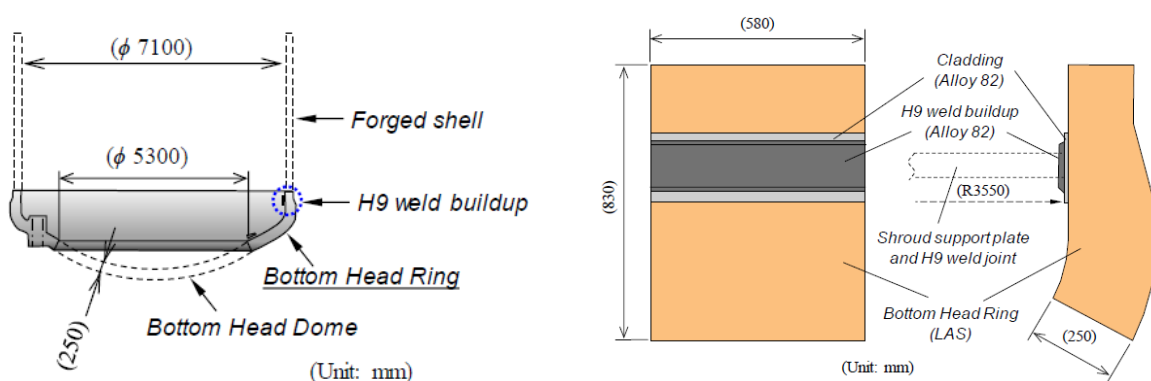


Figure 1. Schematic drawings of RPV bottom head component (left) and test material with H9 weld buildup (right). (referred from Hayashi et al., 2021)

## MECHANICAL PROPERTIES TESTS

### *Mechanical Properties of LAS Base Metal and HAZ*

Tensile tests and elastic-plastic fracture toughness ( $J_{Ic}$ ) tests were conducted. Test specimens were taken from H9 weld buildup location including the adjacent cladding and LAS materials. In order to evaluate mechanical properties of the heat affected zone (HAZ) in the DMW, the center of axis of the tensile specimens and the crack tip locations of the C(T) specimens were designed and controlled. Tensile and C(T) specimens for LAS base metal were taken from the location of a quarter of thickness of bottom head ring near H9 weld buildup. The location of specimen preparation and mechanical properties test results are provided in the previous reports (Hayashi et al., 2021 and Ogawa et al., 2023). Note that the crack orientation in the fracture toughness tests was designed to be equivalent to an axial crack of the RPV bottom head ring.

### *Mechanical Properties of Cladding*

Tensile and  $J_{Ic}$  tests were conducted for cladding, as well as LAS base metal and the HAZ. Figure 2 shows locations of specimen preparation for cladding. The center of axis of the tensile specimens and the crack tip locations of the C(T) specimens were set as distance of 5 mm from the fusion line. The crack orientation in the fracture toughness tests was equivalent to an axial crack of the RPV bottom head ring, as well.

Tensile tests were performed at room temperature (R.T.) in accordance with JIS Z 2241. Round-bar specimen with a diameter of 3 mm was used. Their axes were in the welding direction (circumferential direction of the RPV bottom head), i.e., the direction parallel to the loading direction in the fracture toughness tests. The tensile test results are shown in Table 1.  $J_{Ic}$  tests were performed at R.T. in accordance with ASTM E1820. 0.6T-C(T) specimen was used. Side grooves were machined after introducing a fatigue pre-crack. The  $J_{Ic}$  test results are shown in Table 2.  $J$ - $\Delta a$  data plots with power-law fitting curve ( $J$ - $R$  curve) were shown in Fig. 3.

## FRACTURE TESTS OF DMW PLATE SPECIMENS

The plate specimens for the fracture tests were taken from the locations of DMW in H9 weld buildup. Figure 4 shows the detailed geometry of the DMW plate specimen. The front side of the test section is alloy 82 and the back side is LAS. To investigate a potential effect of crack tip locations in the HAZ on the fracture behavior of DMW plate, the thicknesses of the alloy 82 weld ( $d_w$ ) and the LAS base metal ( $d_b$ ) were designed and controlled when preparing the specimens. Three specimens having different  $d_w$  and  $d_b$  were prepared as shown in Table 3. A semi-elliptical surface flaw was introduced at the center of the plate width and plate length by electrical discharge machining (EDM), followed by fatigue pre-cracking. The depth and length of the fatigue pre-crack are shown in Table 3. The depth of the fatigue pre-crack was measured on the fracture surface after the test and corrected since the plate thickness was reduced due to the plastic deformation during the fracture test. All the DMW plate specimens had crack fronts in the HAZ at the deepest point and in alloy 82 weld metal at the surface points. Note that detail of the DMW plate specimen preparation and the results of fracture tests and fracture surface observations were provided in the previous report (Hayashi et al., 2021).

This paper describes the fracture test results for the DMW plate specimens concisely. Figure 5 shows relationship between load and CMOD for the DMW plate specimens. Despite differences in the  $d_w$  and  $d_b$ , almost the same load-CMOD relationship and the fracture loads (maximum loads) were obtained. Note that the fracture tests were conducted under a periodic unloading condition to use the change of the compliance during unloading for evaluation of the fracture resistance characteristic for the plate specimens.

Table 1: Tensile test results for cladding.

Material	Specimen location	Distance from fusion line (mm)	$\sigma_{0.2}$ (MPa)	$\sigma_f$ (MPa)	$\epsilon_f$ (%)	$\varphi$ (%)
Alloy 82	Weld metal	5	377	597	49	57
			367	596	49	65

Table 2: Fracture toughness test results for cladding.

Specimen ID	Material	Crack tip location	Distance from fusion line (mm)	$J_{Ic}$ (kJ/m <sup>2</sup> )	Validity for $J_{Ic}$
LS5-1	DMW	Weld metal	5	496	Valid
LS5-2				606	Valid

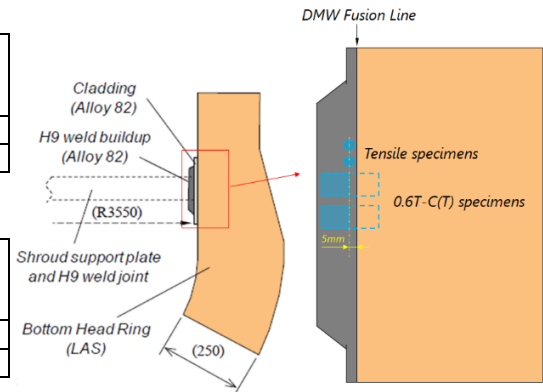
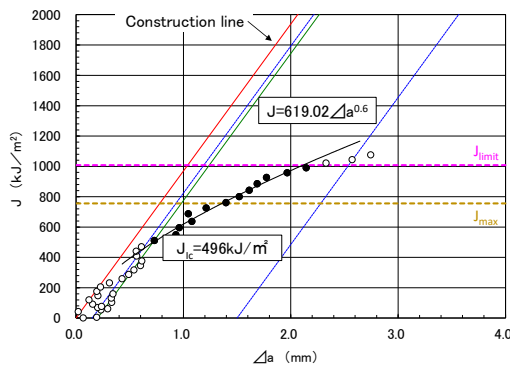


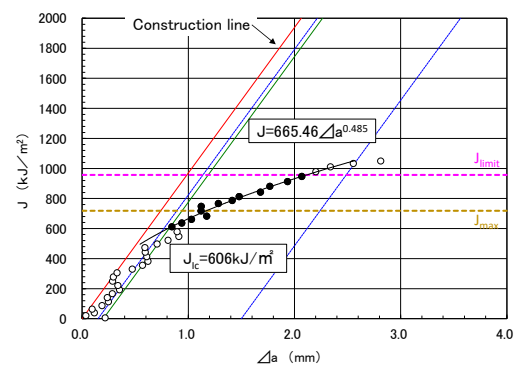
Figure 2. Specimen preparation for cladding.

Table 3: Dimensions of fatigue pre-cracks and thicknesses for DMW plate specimen.

Plate ID	Material	Dimensions of fatigue pre-cracks			Dimensions of thicknesses	
		$a$ (mm)	$2c$ (mm)	$a/c$	$d_w$ (mm)	$d_b$ (mm)
LH-AW4	A82/LAS (DMW)	11.2	28.0	0.20	4	16
LH-AW6		10.5	28.2	0.19	6	14
LH-AW8		10.5	27.8	0.19	8	12



(a) Specimen LS5-1



(b) Specimen LS5-2

Figure 3.  $J$ - $\Delta a$  data and fitting curves for cladding.

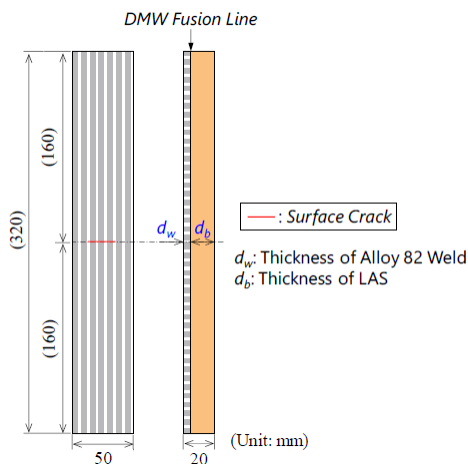


Figure 4. Geometry of DMW plate specimen. (referred from Hayashi et al., 2021)

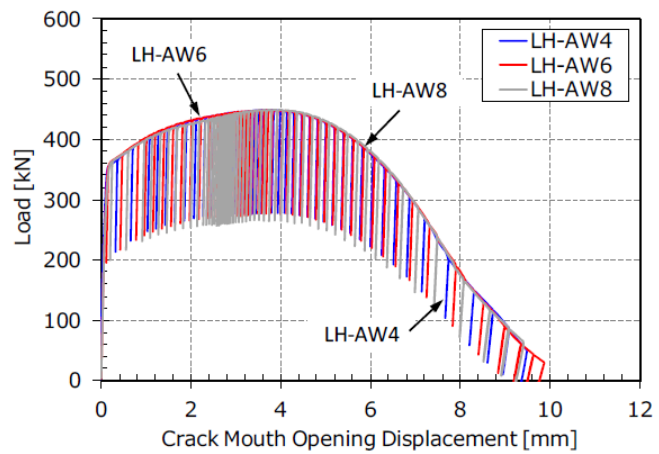


Figure 5. Load-CMOD relationship for DMW plate specimen. (referred from Hayashi et al., 2021)

## FRACTURE ANALYSIS

### GTN Model

In this study, GTN model (Gurson, A. L., 1977, Tvergaard V., 1981), which can analyse ductile fracture behavior due to nucleation, growth, and coalescence of voids in metallic materials, was applied for fracture analysis. The GTN model is described below.

$$\Phi = \left(\frac{\sigma_{eq}}{\sigma_0}\right)^2 + 2f^*q_1 \cosh\left(\frac{3}{2} \frac{q_2 \sigma_m}{\sigma_0}\right) - (1 + q_3 f^{*2}) = 0 \quad (1)$$

Here,

$$\begin{aligned} f^* &= f & \text{for } f &\leq f_c \\ f^* &= f_c + K(f - f_c) & \text{for } f &> f_c \end{aligned} \quad (2)$$

$$K = \frac{1/q_1 - f_c}{f_F - f_c} \quad (3)$$

The total void volume change is given by the equation below.

$$\dot{f} = \dot{f}_{gr} + \dot{f}_N \quad (4)$$

$$\dot{f}_{gr} = (1 - f)\dot{\epsilon}^{pl} \quad (5)$$

$$\dot{f}_N = A\dot{\epsilon}_m^{pl} \quad (6)$$

$$A = \frac{f_N}{S_n \sqrt{2\pi}} \exp\left(-\frac{1}{2} \left(\frac{\bar{\epsilon}_m^{pl} - \epsilon_n}{S_n}\right)^2\right) \quad (7)$$

There are nine parameters  $q_1, q_2, q_3, f_0, f_c, f_F, f_N, S_n$  and  $\epsilon_n$ . Since  $q_3$  is normally equal to  $q_1^2$ , it is needed to determine eight parameters for simulations using the GTN model. In the present study, the GTN model parameters were determined based on the results of fracture toughness tests using C(T) specimen. Then, the fracture analyses for the DMW plate specimens were conducted by using the GTN model parameters determined. The commercial FEA code ‘‘ABAQUS ver. 2017’’, which incorporates the GTN model, was used for simulation. Explicit analysis was performed to consider the extensions of ductile crack during the fracture tests.

### Determination of GTN Model Parameters

The GTN model parameters were investigated for alloy 82 weld (cladding) and LAS, respectively. Fracture analyses for C(T) specimens were performed to determine the GTN model parameters. Figure 6 shows an example of the FEA model for C(T) specimen. A quarter model was applied. The element type was C3D8R. Quarter sector of the loading pin was modelled, simulating a rigid pin by applying significantly high elastic modulus compared with that of the specimen. As described below, several kinds of C(T) specimen size (0.6T-C(T), 0.7T-C(T) and 0.8T-C(T)) were used for  $J_{Ic}$  tests. Despite the size of the C(T) specimen, the minimum element size near the crack tip was set 0.1 mm. Detail of parameters investigation for the LAS base metal was provided in the previous report (Ogawa et al., 2023). Table 4 shows the GTN model parameters. It was confirmed that a simulation using the GTN model can reproduce relationship between load and load-line displacement (LLD) obtained in the fracture toughness test, as shown in Fig. 7.

DMW plate specimen shown in Fig. 4 includes HAZ as well as LAS base metal and alloy 82 cladding. To define material properties including the GTN model parameters for the HAZ, the applicability of the material properties of LAS base metal was investigated. In the previous report (Hayashi et al., 2021),

the authors have performed several  $J_{Ic}$  tests using C(T) specimens under controlling the fatigue pre-crack tip locations in the HAZ. Figure 8 compares  $J_{Ic}$  test result, in which the pre-crack tip is in the HAZ and the distance from the fusion line to the pre-crack tip is approximately 2 mm, with analysis result using the GTN model parameters for the LAS base metal. Note that the maximum load in Fig. 8 is quite different from that in Fig. 7 due to a difference in size of the C(T) specimen. Analysis using the GTN model parameters for the LAS base metal provided a good prediction of the load-LLD relationship in the HAZ. It is considered reasonable to apply the material properties for LAS base metal to the HAZ region as an engineering approach.

Fracture analysis for 0.6T-C(T) specimen was performed to investigate the GTN model parameters for alloy 82 weld. Young's modulus of 200,000 MPa and Poisson's ratio of 0.3 were applied. The true stress–true plastic strain relationship up to the uniform elongation obtained by the tensile test was extrapolated based on ISO 27306:2016 Annex B. Although the GTN model parameters  $q_1$  and  $q_2$  of 1.5 and 1.0 are commonly applied, those parameters were determined based on the 0.2% proof stress and work hardening exponent of the test material by reference to Faleskog et al., 1998. The parameters  $q_1$  and  $q_2$  determined were 1.66 and 0.98, respectively. The GTN model parameters determined for alloy 82 weld were also shown in Table 4. Figure 9 compares test result of specimen LS5-2 with analysis result using the GTN model parameters determined. Difference in loads between the test and analysis is relatively large, compared with Fig. 7 for LAS base metal. Note that there appears to be a possibility to improve the parameters for alloy 82 weld.

Table 4: GTN model parameters determined.

Material	$q_1$	$q_2$	$q_3$	$f_0$	$f_c$	$f_F$	$\epsilon_n$	$s_n$	$f_N$
LAS (base metal)	1.70	0.85	2.87	$10^{-5}$	0.035	0.28	0.5	0.1	0.06
Alloy 82 (weld)	1.66	0.98	2.76	$10^{-4}$	0.2	0.4	0.5	0.1	0.06

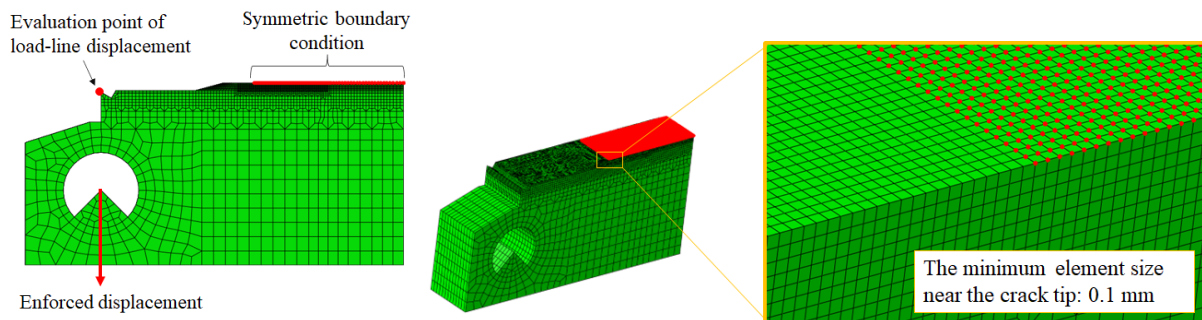


Figure 6. FEA model for C(T) specimen (referred from Ogawa et al., 2023).

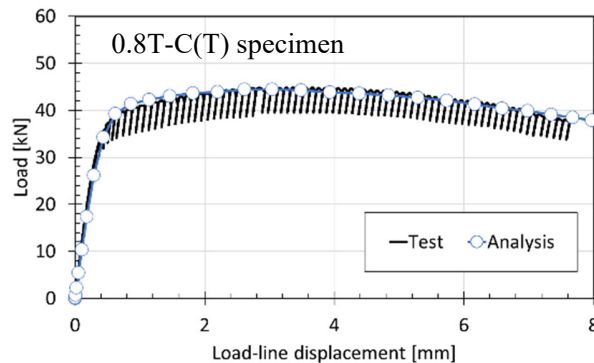


Figure 7. Comparison of load-LLD relationship for LAS base metal between test and analysis. (referred from Ogawa et al., 2023)

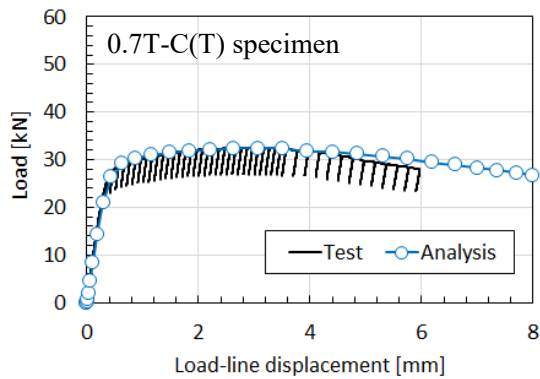


Figure 8. Comparison of load-LLD relationship between test for HAZ and analysis using material parameters for LAS base metal.

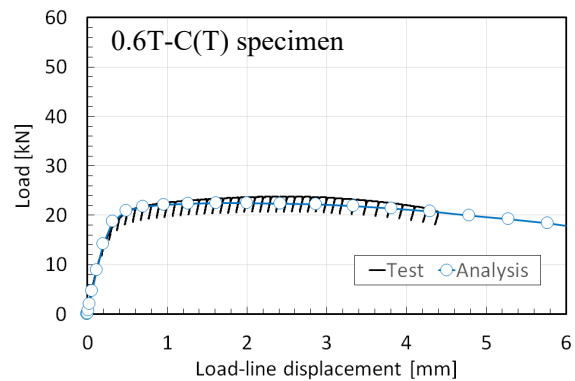


Figure 9. Comparison of load-LLD relationship for alloy 82 weld between test and analysis.

### **Fracture Analysis for DMW Plate Specimens**

Analyses for the DMW plate specimens were investigated by using the GTN model parameters determined. As shown in Fig. 5, all the three DMW plate specimens were tested. In this paper, fracture analysis for a DMW plate specimen (LH-AW8) was presented, representatively, since the load-CMOD relationship and the fracture loads were almost the same among all the three DMW plate specimens. Figure 10 shows FEA model for the DMW plate specimen. Same as the FEA model for C(T) specimen, a quarter model, the element type of C3D8R and the minimum element size of 0.1 mm were applied. The material properties such as Young's modulus, Poisson's ratio, stress-strain relationship and GTN model parameters for LAS base metal and alloy 82 weld were applied, respectively. Enforced displacement was applied on the edge surface of the plate specimen.

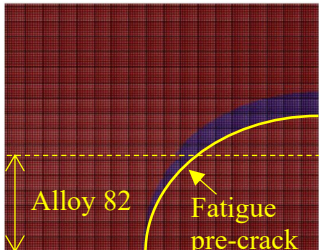
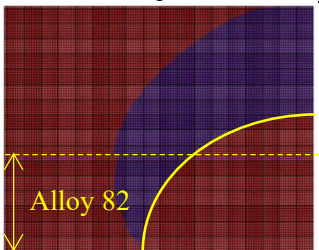
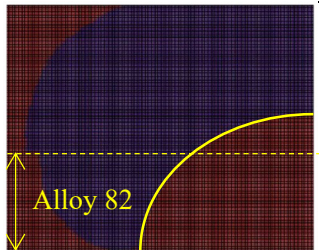
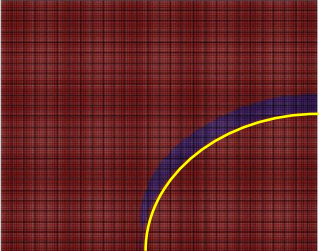
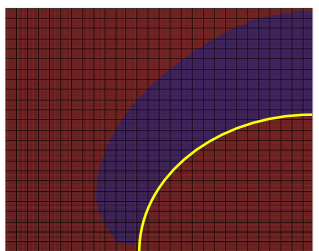
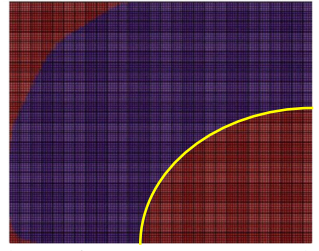
Figure 11 compares load-CMOD relationship by the FEA with that by the fracture tests. Two kinds of fracture analyses were performed. In one case, material properties for LAS base metal and alloy 82 weld were applied to each region (Case-1). In the other case, only material properties for LAS base metal were applied to all the FEA model as a simplified analysis condition (Case-2). In the range up to the maximum load, FEA Case-1 provided slightly lower loads than the test results, while Case-2 provided slightly higher loads. The maximum loads obtained by Case-1 and Case-2 were 450 kN and 469 kN, respectively, against 449 kN of the maximum load by the test. At the point of view of the estimation of the maximum load (fracture load), Case-1 showed remarkably good estimation, though the estimation error for Case-2 was not so large. In the range after the maximum load, decrease of the load due to ductile crack extension was observed, and Case-1 provided slightly higher load than Case-2 in this range. Points of the thickness penetration of the ductile crack in the test and analyses were also shown in Fig. 11. The thickness penetration in the test was visually judged by using the video recording on the back surface of the DMW plate specimen. On the other hand, those in the analyses were evaluated based on the contour plots of the ductile crack extension. It was found that the thickness penetrations in the FEA were almost corresponding to that in the fracture test.

### **Discussion**

Fracture surface of the DMW plate specimen was shown in Fig. 12. Contrary to the relatively flat fracture surface extending from the pre-crack front to the back side of the specimen in the depth direction was observed. Here, note that the ductile crack extension under loading occurred preferentially in the depth direction without noticeable extensions at surface points. Crack extension in the length direction on the

specimen surface occurred after crack penetration. Ductile crack extension behavior obtained by FEA at near the maximum load, thickness penetration and fracture were summarized in Table 5. Blue area indicates region where ductile crack extension occurred. Significant difference in ductile crack extension behavior was not found between Case-1 and Case-2. Similar behavior as the fracture surface, that was preferential ductile crack extension in the crack depth direction without noticeable extensions at surface points, was observed from both FEA results. In Case-1, discontinuity of the ductile crack front due to a difference in the material properties was found. It was considered that the difference in the material properties, especially  $f_0$ ,  $f_c$  and  $f_F$ , caused relatively high resistance for ductile crack extension in alloy 82 region. By comparison with Case-2, it was considered Case-1 provided lower load because Case-1 considered the material properties for alloy 82 weld whose yield stress was lower than that of LAS (see Hayashi et al., 2021) in the range up to the maximum load. On the other hand, it was considered Case-1 provided higher load due to relatively high resistance for ductile crack extension in alloy 82 in the range after the maximum load. In conclusion, it was considered that FEA simulation using the GTN model can predict the load-CMOD relationship and ductile crack extension behavior with a practical accuracy. These results strongly support the applicability of the GTN model to fracture evaluation for the DMW in a RPV bottom head component of BWR.

Table 5: Ductile crack extension behavior obtained by FEA.

FEA/Test	Maximum load	Thickness penetration	Fracture
FEA Case-1	 ( $P=450$ kN, CMOD=4.9 mm)	 ( $P=309$ kN, CMOD=7.3 mm)	 ( $P=95$ kN, CMOD=9.3 mm)
FEA Case-2	 ( $P=469$ kN, CMOD=4.7 mm)	 ( $P=296$ kN, CMOD=7.2 mm)	 ( $P=38$ kN, CMOD=9.4 mm)

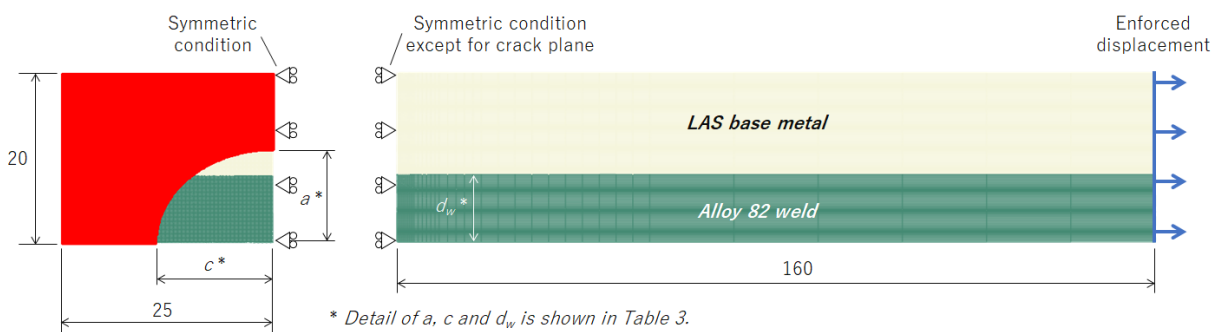


Figure 10. FEA model for DMW plate specimen.

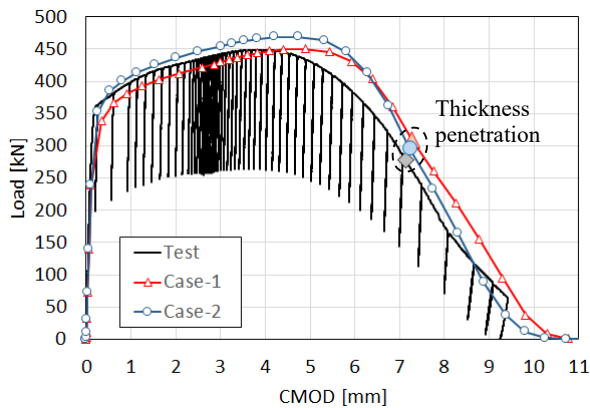


Figure 11. Comparison of load-CMOD relationship for DMW plate specimen LH-AW8.

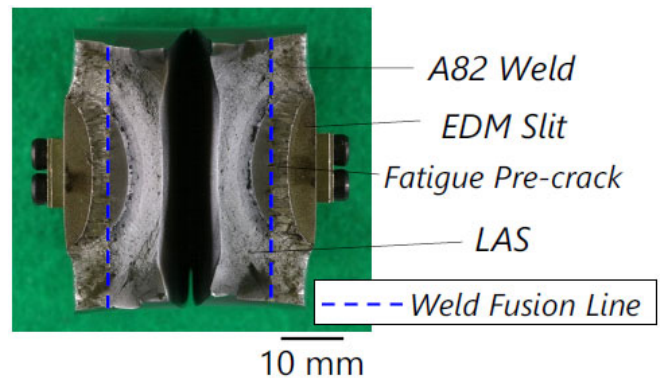


Figure 12. Fracture surface of DMW plate specimen. (LH-AW8)

## NOMENCLATURE

BWR	boiling water reactor	RPV	reactor pressure vessel
SCC	stress corrosion cracking	GTN	Gurson-Tvergaard-Needleman
LAS	low alloy steel	DMW	dissimilar metal weld
EPFM	elastic-plastic fracture mechanics	C(T)	compact tension
CMOD	crack mouth opening displacement	FEA	finite element analysis
HAZ	heat affected zone	LLD	load-line displacement
$\Delta a$	amount of ductile crack extension	$a$	depth of surface flaw
$2c$	length of surface flaw	$a/c$	aspect ratio of surface flaw
$d_w$	thickness of alloy 82 weld	$d_b$	thickness of base metal
$P$	load	$K_{Ic}$	plane strain fracture toughness
$J_{Ic}$	elastic-plastic fracture toughness	$\sigma_0$	yield stress
$\sigma_{eq}$	von Mises equivalent stress	$\sigma_m$	hydrostatic stress
$\sigma_{0.2}$	0.2% proof stress	$\sigma_u$	ultimate tensile strength
$\varepsilon_f$	elongation	$\varphi$	reduction of area
$f$	void volume fraction	$f_0$	initial void volume fraction
$f_c$	critical void volume fraction	$f_F$	void volume fraction at final failure
$s_n$	strain at void nucleation (standard deviation)	$\varepsilon_n$	strain at void nucleation (mean)
$f_N$	void volume fraction at nucleation	$\Phi$	yield function
$q_1, q_2, q_3$	material parameters of GTN model		

## CONCLUSION

The applicability of damage mechanics analysis by using GTN model to fracture evaluation for the DMW of RPV bottom head components consisted of Ni-base alloy weld metal and LAS was investigated.

- (1) The GTN model parameters, which can reproduce load-LLD relationship of fracture toughness tests using C(T) specimen, were determined for LAS base metal and alloy 82 weld. It was considered reasonable to apply the material properties for LAS base metal to the HAZ region as an engineering approach.
- (2) Analysis using the GTN model can predict the load-CMOD relationship and ductile crack extension behavior for the DMW plate fracture test with a practical accuracy. These results strongly support the

applicability of the GTN model to fracture evaluation for the DMW in a RPV bottom head component of BWR.

## REFERENCES

- Bamford, W. and Hall, J. (2003). "A Review of Alloy 600 Cracking in Operating Nuclear Plants: Historical Experience and Future Trends." *11th International Conference on Environmental Degradation of Materials in Nuclear Systems – Water Reactors*; pp. 1071-1081. Stevenson, WA, August 10-14.
- Matsunaga, T. and Matsunaga, K. (2003). "Stress Corrosion Cracking of CRD Stub Tube Joint and Repair at Hamaoka Unit 1." *11th International Conference on Nuclear Engineering, ICONE-36056*.
- Aoki, T., Hattori, S., Anzai, H. and Sumimoto, H. (2005). "Stress Corrosion Cracking in Ni-base Alloy Used for a Long Time in a BWR." *Maintenology* Vol. 4, No. 1: pp. 34-41.
- Bjurman, M., Jädernäs, D., Kese, K., Jenssen, A., Chen, J., Cocco, M. and Johansson, H. (2017). "Root Cause Analysis of Cracking in Alloy 182 BWR Core Shroud Support Leg Crack." *18th International Conference on Environmental Degradation of Materials in Nuclear Power Systems - Water Reactors*: pp. 819-829. Portland, OR, August 13-17.
- Nuclear Regulatory Commission (NRC), (2017). "Limerick Generating Station, Unit 2 – Relief Request 14R-17, Associated with the Alternate Repair of a 2-inch Instrument Line Nozzle at Penetration N-16D on the Reactor Pressure Vessel (CAC NO. MF9702)," *ADAMS Accession No: ML17208A090*, August 14.
- Case N-749 (2012). "Alternative Acceptance Criteria for Flaws in Ferritic Steel Components Operating in the Upper Shelf Temperature Range, Section XI, Division 1." *ASME Boiler and Pressure Vessel Code*.
- Gustin, H. L., Cipolla, R. C., Xu, S. X. and Scarth, D. A. (2012). "Alternative Acceptance Criteria for Flaws in Ferritic Steel Components Operating in the Upper Shelf Temperature Range." *Proceedings of the ASME 2022 Pressure Vessels & Piping Conference, PVP2012-78190*.
- Hayashi, T. et al. (2021). "Study on Fracture Behavior and Assessment for Dissimilar Metal Weld of Low Alloy Steel and Ni-base Alloy Weld Using a BWR Reactor Pressure Vessel Material", *Proceedings of the ASME 2021 Pressure Vessels & Piping Conference, PVP2021-61467*.
- Hayashi, T. et al. (2022). "Study on Ductile Crack Extension and Fracture Behavior in Plate Specimen with a Semi-elliptical Surface Crack Using a BWR Reactor Pressure Vessel Material", *Proceedings of the ASME 2022 Pressure Vessels & Piping Conference, PVP2022-84606*.
- Yoshida S. et al., (2022). "Study on Fracture Assessment for BWR Reactor Pressure Vessel Steel by GTN model", *The Japan Society of Mechanical Engineers M&M2022 conference, OS0111*.
- Ogawa, T. et al. (2023). "Study on the Applicability of GTN Model on Fracture Evaluation for Plate Specimen with a Surface Crack Using a BWR Reactor Pressure Vessel Material", *Proceedings of the ASME 2023 Pressure Vessels & Piping Conference, PVP2023-107208*.
- Gurson, A. L. (1977), "Continuum Theory of Ductile Rupture by Void Nucleation and Growth: Part I – Yield Criteria and Flow Rules for Porous Ductile Materials", *Journal of Engineering Materials and Technology*, vol. 99, pp. 2-15.
- Tvergaard V. (1981), "Influence of Voids on Shear Band Instabilities under Plane Strain Conditions", *International Journal of Fracture*, Vol. 17, pp. 389-407.
- ISO 27306:2016 (2016), "Metallic Materials – Method of Constraint Loss Correction of CTOD Fracture Toughness for Fracture Assessment of Steel Components".
- Faleskog, J. et al. (1998), "Cell Model for Nonlinear Fracture Analysis – I. Micromechanics Calibration", *International Journal of Fracture*, Vol. 89, pp. 355-373.